THE ARCHIVE OF MECHANICAL ENGINEERING

VOL. LIV 2007 Number 4

DOI: 10.24425/ame.2007.131560

Key words: shell, constrained torsion, open cross section, post buckling, finite elements method

TOMASZ KOPECKI [*], *HUBERT DĘBSKI* [**]

BUCKLING AND POST-BUCKLING STUDY OF OPEN SECTION CYLINDRICAL SHELLS SUBJECTED TO CONSTRAINED TORSION

The work concerns numerical – experimental studies on pre- and post-buckling of thin-walled, steel, cylindrical shells, with the open section, subjected to constrained torsion. Two geometrically varied structures are considered: an open section cylindrical shell without stiffeners and one that is reinforced by closed section stringers. The shells have five different length to diameter ratios. Numerical simulations were carried out and the neuralgic zone stress distributions in pre- and post-buckling responses, were determined. Torsion experiments were performed and the results were compared to the numerical conclusions, with reasonably high level of agreement. The exactness of the experiment was proven for selected cases, establishing the basis for FEM numerical model estimation.

1. Introduction

The demand for light-weight and high-strength structures, assuming a reasonable pay load to dead weight relation, has led to ongoing research, into more efficient computation methods and testing of new structures. This trend can be observed in the majority of technological fields, in particular in those, where a thin-walled structure is necessary. Structural durability and reliability are determined by the presence of neuralgic zones, which have to support functionality. These zones provide an area of lesser strength, where stress may be concentrated and commonly introduce abrupt variations of geometric parameters. While it is not difficult to obtain the required torsional rigidity for closed section shell structures, to meet this condition in the case of open section structures, is considerably more complex [7], [9], [11], [12].

[*] *Faculty of Mechanical Engineering and Aeronautics, Rzeszów University of Technology, ul. W. Pola 2, 35-959 Rzeszów; E-mail: t_kopecki@wp.pl*

[**] *Faculty of Mechanical Engineering, Lublin University of Technology, ul. Nadbystrzycka 36, 20-618 Lublin; E-mail: h.debski@pollub.pl*

In such cases, one of the most frequently used methods to obtain the required torsional rigidity, is to enforce the boundary conditions through clamping, at least one of the free cross section ends. As a result, normal stress appears in the cross section, in addition to the shear stress. This kind of loading, defined as constrained torsion, leads to the existence of high level stress gradients, which appear, in particular, at the free lengthwise border of the shell. This could reduce the fatigue life of the structure and its load capacity. It is therefore necessary to strengthen the lengthwise boundaries, usually by applying closed cross section stringers.

In our paper, the problem will be considered, using the example of open section shell structures, subjected to constrained torsion.

2. Subject and scope of the study

The subject to be considered, concerns numerical-experimental analysis of open cross section, thin-walled cylindrical shells, subjected to constrained torsion. The range of numerical calculations includes pre- and post-buckling stress analysis and determination of critical loads. Two geometrically varied structures are considered. The first is an open section cylindrical shell without stiffening. The second structure represents the shell reinforced by three stringers of closed section. Five different length to diameter ratios are taken into account: L/D = 1.0, 2.0, 3.0, 4.0, 5.0.

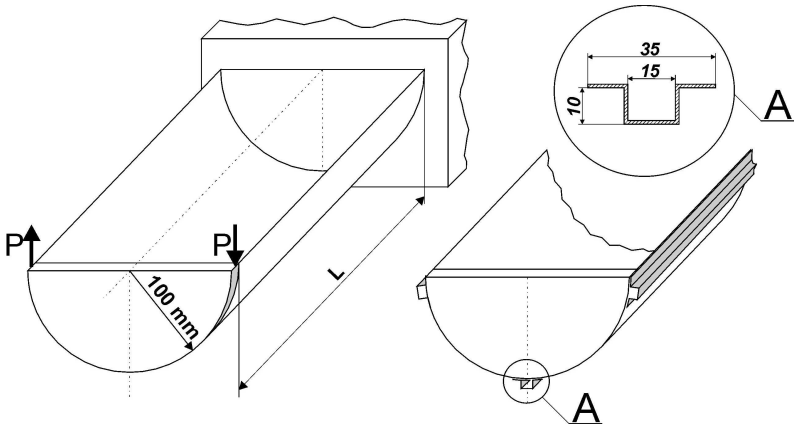

Fig. 1. Installation, loading device and dimensions of the cross section

Parallel to the numerical computations, for two of the variants mentioned above, actual experiments were performed: one on the shell without stiffening, and one on the shell which had been reinforced by three closed section stringers. A ratio of L/D = 5 was assumed in both cases.

The installation, loading device and structure dimensions, with reinforcing stringers cross section is shown in Fig. 1.

3. Finite element – linear analysis of pre-buckling and buckling

Although elastic buckling analysis of the structures is generally a nonlinear problem, in a number of cases, important from a practical point of view, pre-buckling and buckling analysis can be performed as a linear system.

The shells, considered in this study, were analysed with the ABACUS finite elements solver [3]. The pre-buckling analysis of the shells, was determined, using the linear static analysis option, and conventional bifurcation buckling analysis was applied. The approach to the buckling prediction is based on the development of a linear perturbation of the structure stiffness about an equilibrium point, which means the initial equilibrium under no load or in a preloaded state. At any time, the structure's total elastic stiffness is

$$[K]^0 + [K]^p \,, \tag{a}$$

where $[K]^0$ is the stiffness presented by the material and $[K]^p$ is the initial stress and load stiffness, caused by non-zero loading. For the elastic systems, $[K]^0$ is almost constant and the variation of $[K]^p$ is proportional to the load variation. During the bifurcation buckling step, there may be a non-zero "dead" load of P and there must be a linear perturbation with load Q, specified in the bifurcation buckling step. The aim of this process is to estimate multiples of Q, which combined with P cause instability.

Since the response is assumed to be elastic, and therefore, closely proportional to load, the stiffness at $P + \lambda Q$ load is well approximated by

$$[K]^0 + [K]^p + \lambda\,[K]^q \,, \tag{b}$$

where $[K]^q$ is the initial stress and load stiffness, caused by Q. Thus, the buckling load estimation is provided by the eigenvalue equation:

$$\left([K]^0 + [K]^p + \lambda\,[K]^q\right)\phi = \{0\} \,. \tag{1}$$

The eigenvalue λ is a multiplier of the applied load, which when added to the preload factor, provides the critical load estimate: the predicted collapse load is $P + \lambda Q$ and ϕ is the collapse mode.

For problems involving buckling behaviour, according to [2] and [3], quadrilateral four node shell elements, with six degrees of freedom, were used in the models. Using MPC-TIE elements, connections of surface and stringers were made in the points of the rivet axises. In order to eliminate

the potential for interpenetrating surfaces, during eventual local buckling between rivets, very low stiffness solid elements were introduced in the space between stringers and surface. To define the boundary conditions corresponding to constrained torsion, translational degrees of freedom were blocked in the nodes of the fixed boundary cross section. Using MPC-PIN standard elements, the opposite boundary sections of the shell were connected with 10 mm thick stiff plates.

At the first step, calculations were used for the structure without stiffeners. The following constants were assumed: Young's modulus $E = 2.1 \cdot 10^5$ [N/mm^2] and Poisson's ratio $v = 0.3$. Assuming the constant shell diameter of $D = 200$[mm], calculations were performed for five values of shell length: L = 200, 400, 600, 800 and 1000[mm]. In all cases the regular grid of structural partition, for rectangular elements was assumed. The number of elements was increased repeatedly, according to the results obtained. In every geometric variant the same size value of the characteristic grid – a, (see picture 2) measured along the structure length, was maintained. FEA shell models: without stiffeners – $L = 200$[mm] – minimal considered length, and with stiffeners – $L = 1000$[mm] – maximum length are presented in Fig. 2.

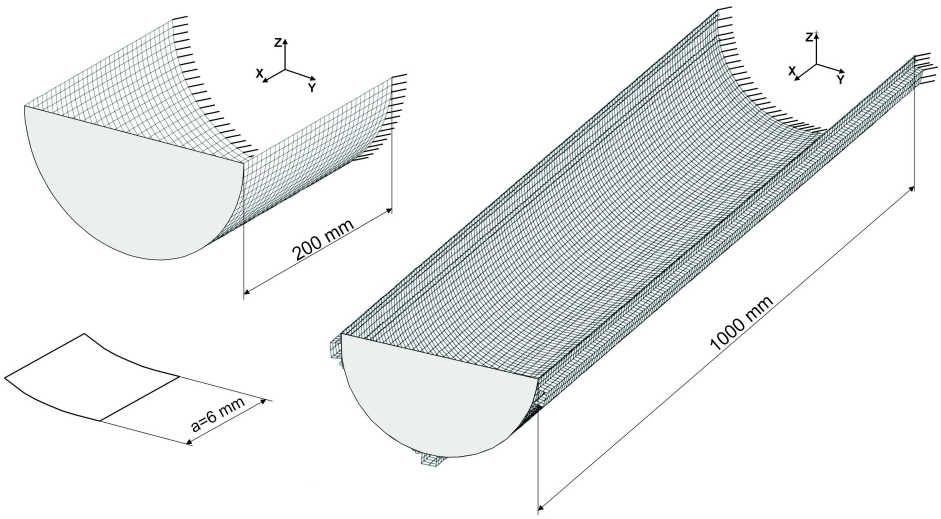

Fig. 2. Two examples of FEA shell models:
a) shell without stiffeners – $L = 200$[mm], b) shell with stiffeners – $L = 1000$[mm]

3.1. Structure without stiffening

In order to determine the stress distribution in a shell without stiffening in the pre-buckling stage, calculations for all geometric variants were performed,

assuming the unitary external loading of $M_t = 0.1$[Nm]. Effective stress distribution, according to Von Mises' criterion is shown in Fig. 3.

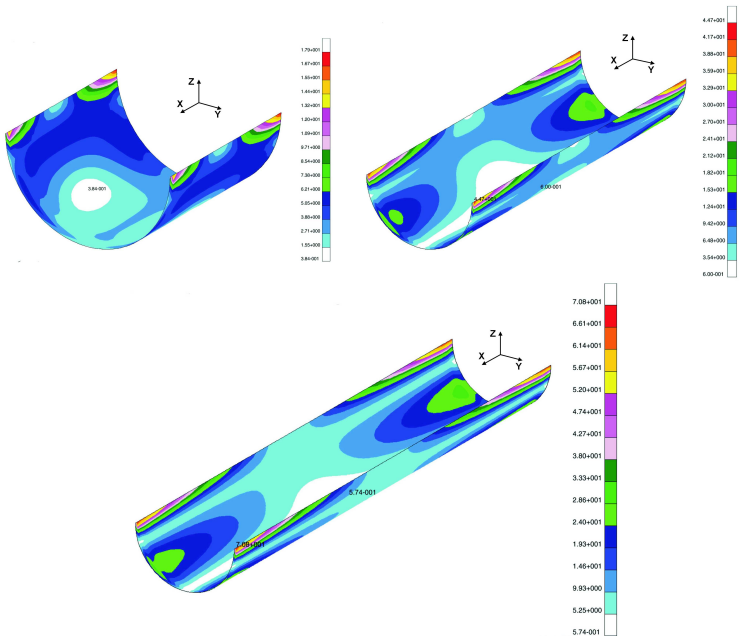

Fig. 3. Effective stress distribution according to Von Mises' criterion in the pre-buckling state. Shells without stiffening: $L = 0.2$[m], $L = 0.6$[m], $L = 1$[m]

Table 1.
Critical load in geometrically varied numerical models; n – denotes number of finite elements

a [cm]	$L = 0.2$[m]		$L = 0.4$[m]		$L = 0.6$[m]		$L = 0.8$[m]		$L = 1$[m]	
	n	M_{cr} [Nm]	n	M_{cr} [Nm]	n	M_{cr} [Nm]	n	M_{cr} [Nm]	n	M_{cr} [Nm]
1.0	832	60.8	1472	28.37	2112	17.68	2752	12.60	3232	10.30
0.7	1480	61.16	2572	28.74	3706	17.93	4841	12.79	5680	10.45
0.6	2262	61.37	4032	28.91	5746	18.05	7462	12.88	8762	10.52
0.5	3270	61.43	6750	29.00	8230	18.12	10710	12.92	12570	10.56
0.4	5128	61.49	9028	29.08	12928	18.18	16829	12.97	19714	10.60

The results show that the highest stress levels and the largest gradient zones are located in the vicinity of the unbounded longitudinal edges, in the areas adherent to boundary cross sections.

Using the bifurcation buckling option, critical load values and corresponding critical collapse modes were determined. In order to estimate the convergent solution in all variants, the number of elements was increased repeatedly.

The results of the calculations are presented in table 1.

On the basis of the obtained results we are able to present the relation between the critical buckling load M_{cr} versus length L of the shell, for the various geometric values (Fig. 4).

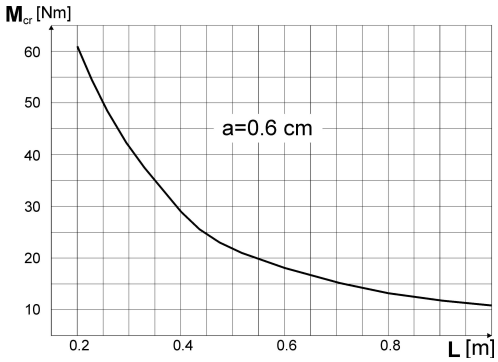

Fig. 4. The critical buckling load M_{cr} versus length L of the shell

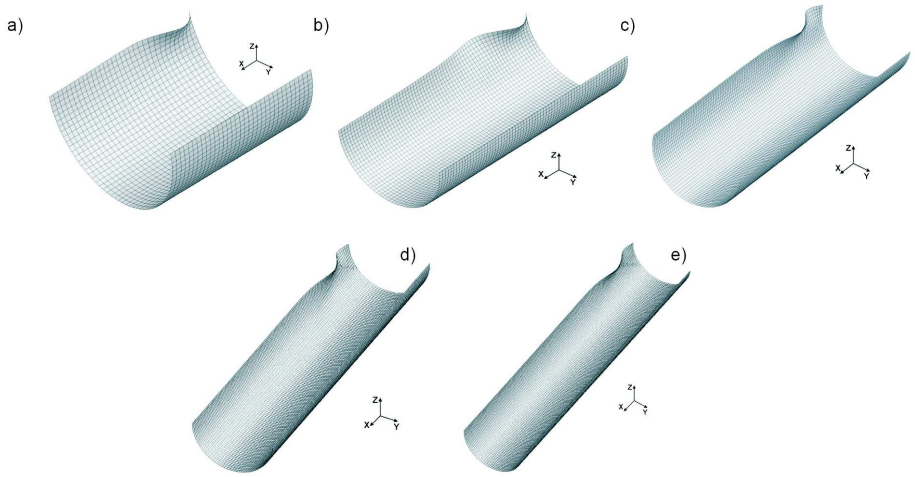

Fig. 5. First buckling modes of geometrically varied numerical models without stiffeners. a) L = 0.2[m], M_{cr} = 61.49[Nm]; b) L = 0.4[m], M_{cr} = 29.08[Nm]; c) L = 0.6[m], M_{cr} = 18.18[Nm]; d) L = 0.8[m], M_{cr} = 12.97[Nm]; e) L = 1[m], M_{cr} = 10.60[Nm]

The numerical results provide a way to represent the shapes of the buckling modes. The first modes for the structures without stiffeners are presented in Fig. 5.

These calculations denote the strongly nonlinear relationship between critical moment and length of shell, if the aspect ratio is $L/D < 2$. Beyond this value, sensitivity of critical moment on the length increment does not considerably increase.

3.2. The structures reinforced by stiffeners

Numerical results obtained for open section shells without stiffeners suggest, that this kind of structure, when subjected to constrained torsion, has

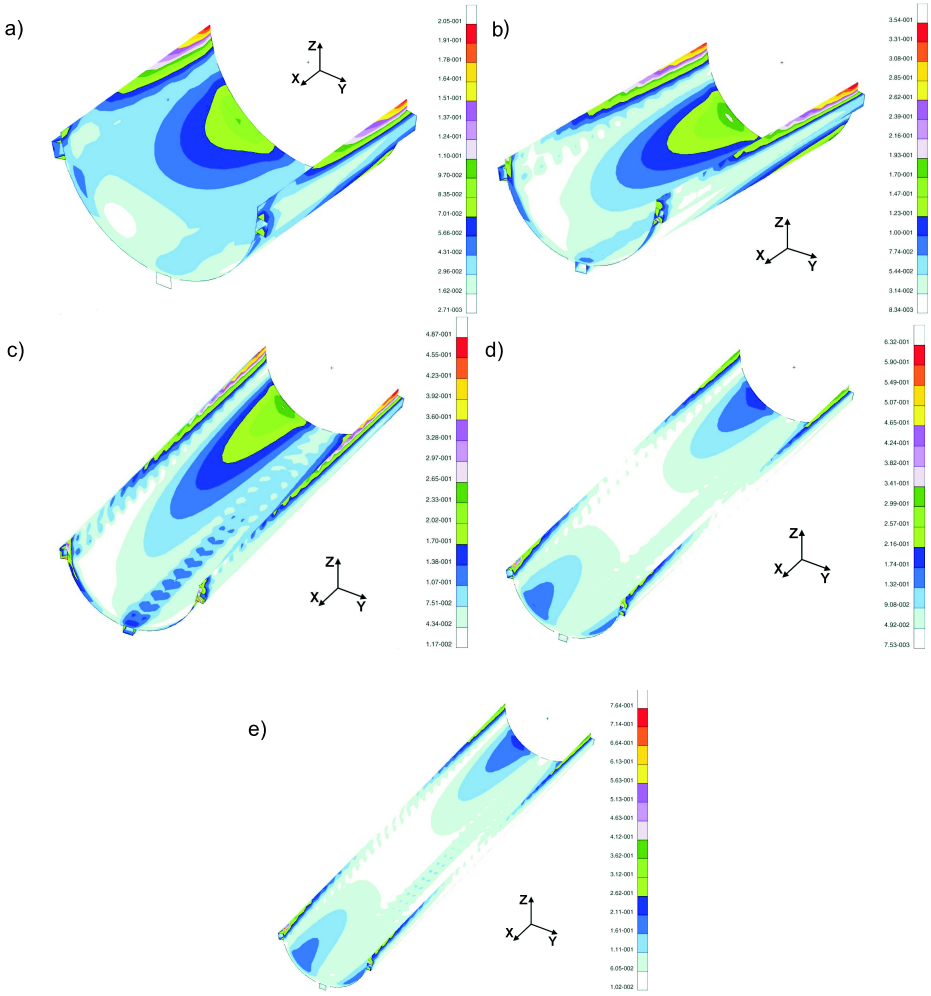

Fig. 6. Effective stress (von Mises) for numerical models with stiffeners, a) $L = 0.2$[m]; b) $L = 0.4$[m]; c) $L = 0.6$[m]; d) $L = 0.8$[m]; e) $L = 1$[m]

no practical application. This is due to an impractically low critical local buckling level, which precludes the possibility of load increase over a critical value. Reinforcing the structure with stringers seems to be an effective way to increase stiffness and capacity. The structures considered in this study were reinforced by thin-wall stringers of closed section. This increased torsional stiffness, in addition to a slight growth in structure weight. In every shell variant, the same stringer cross section geometry, dimensions and quantity, were assumed. Analogically, as in the case of a shell without stiffeners, assuming the unitary external loading factor $M_t = 0.1$[Nm], the character of the stress distribution in the pre-buckling state was determined at the first step. The results of the calculation in the form of effective stress distribution plots, according to von Mises' criterion, is shown in Fig. 6.

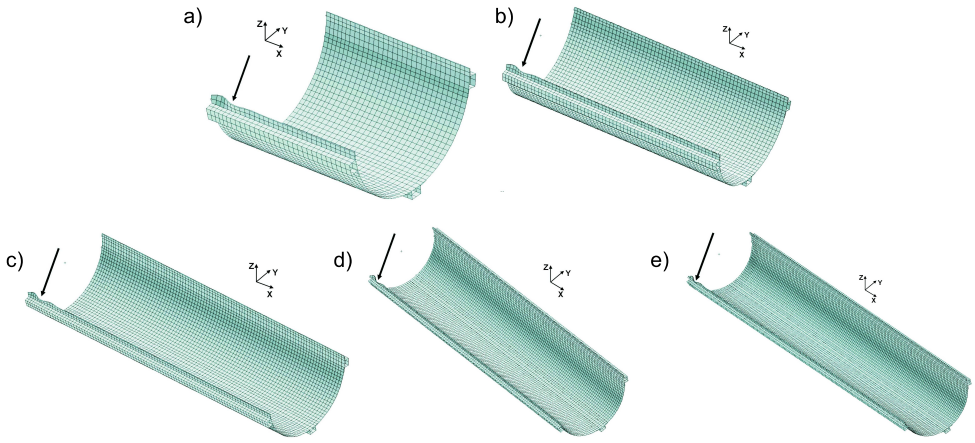

Fig. 7. First buckling modes of geometrically varied numerical models with stiffeners. a) $L = 0.2$[m], $M_{cr} = 184.1$[Nm]; b) $L = 0.4$[m], $M_{cr} = 102.8$[Nm]; c) $L = 0.6$[m], $M_{cr} = 88.3$[Nm]; d) $L = 0.8$[m], $M_{cr} = 84.8$[Nm]; e) $L = 1$[m], $M_{cr} = 82.7$[Nm]

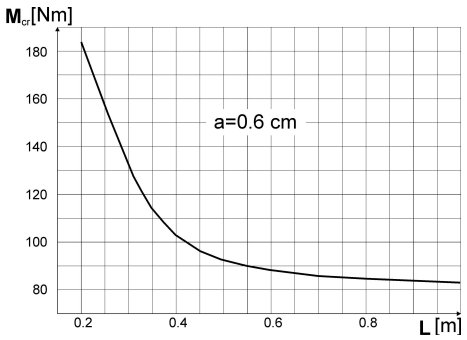

Fig. 8. The critical buckling load M_{cr} versus length L

For a geometric structure with the corresponding load from above, critical moments of M_{cr} and first buckling modes were determined. The shapes of the first buckling modes are shown in Fig. 7.

The effect of length L on the buckling load M_{cr} for the five geometric variants is shown in Fig. 8.

4. Actual Experiments

Parallel to the numerical calculations, qualitative experimental testing was performed on selected variants of the structure. This provided a method for comparison of buckling shape and critical load values obtained in the numerical manner. The experiment was carried out on a special station, able to provide the assumed loading and boundary conditions. Two cases were considered: the shell without reinforcement, and a structure with three stringers of closed section. In both cases the specimen length was $L = 1$[m]. Figure 9 shows the design of this device.

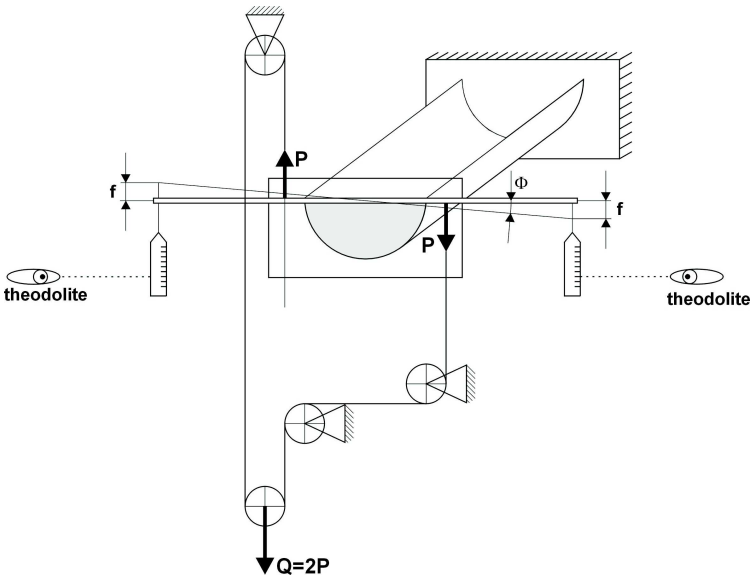

Fig. 9. The experiment device

Structure stiffness measurements in the pre-buckling state range preceded the buckling test. The plot of torsion angle versus torsion moment is shown by Fig. 10.

Fig. 10 shows, in the range of pre-buckling, that the load relationship between torsion moment and torsion angle is linear, exactly up to the moment of abrupt variation.

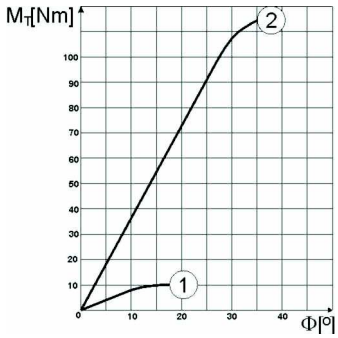

Fig. 10. Torsion angle versus torque moment.
1 – shell without reinforcement, 2 – structure with stiffeners

The local buckling shape of the shell without reinforcement is shown in Fig. 11. In this case, the critical moment is $M^e_{cr} \cong 12.5$[Nm], while the numerical result was $M_{cr} = 10.6$[Nm]. A quantitative comparison of these results suggests reasonably high compatibility ($\sim$ 15%).

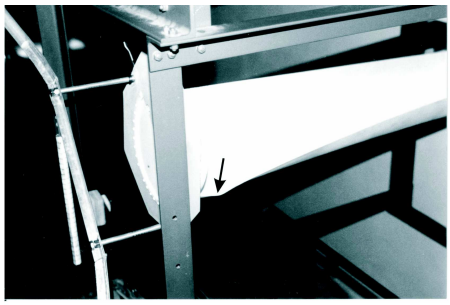

Fig. 11. Local buckling of the structure without reinforcement; $L = 1$[m]

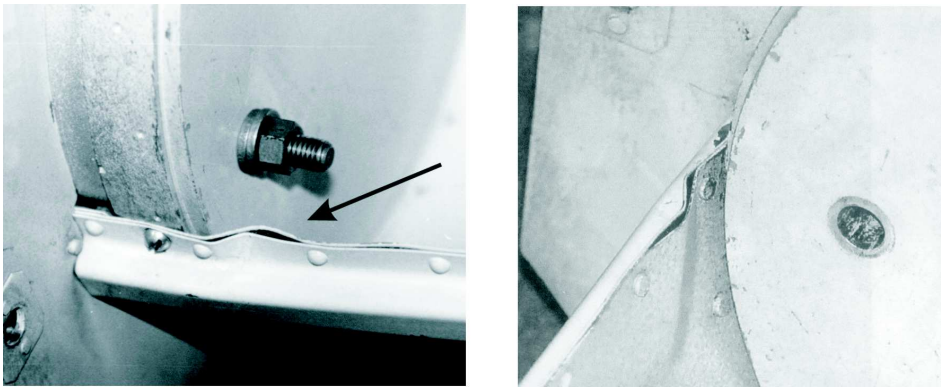

Fig. 12. Post-buckling plastic deformation. Structure reinforced by closed section stiffeners

A similar statement can be made with reference to the test with a reinforced structure. In this case, the critical loading obtained experimentally was also higher than that in the numerical calculation. Post buckling deformation is shown by Fig. 12.

These experiments show that the structures considered are characterised not only by low torsional rigidity, but also by large deformations. Therefore application of the linear FEM analysis can only refer to the under-critical deformation range. It provides a way to identify stress concentration zones, possibly local buckling areas.

In order to determine the stress distribution in the post-buckling state, nonlinear static analysis was done. The stress-strain relation of uniaxial tension for actual material was simplified by the model of the ideal elastic – plastic body with a yield point of 240[MPa] (Fig.13).

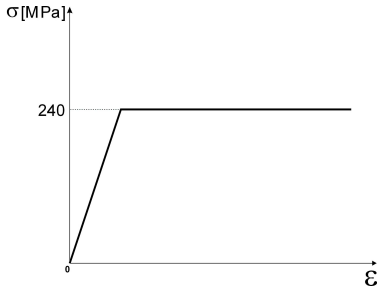

Fig. 13. Stress-strain relation of idealised material

5. Nonlinear FEM analysis

The results of the experiments showed that even a small load increment over the critical value leads to local plastic deformation. Numerical simulation of post-buckling deformation requires a nonlinear application. Large deformations and the change of the structure's rigidity have to be taken into consideration.

Nonlinear formulation of the problem is managed by the discrete equilibrium equations encountered in nonlinear static structural analysis, formulated by the displacement method, presented in the compact force residual form [8]

$$\mathbf{r}(\mathbf{u},\mathbf{\Lambda}) = \mathbf{0}. \tag{2}$$

Here $\mathbf{u}$ is the state vector, containing the degrees of freedom that characterize the configuration of the structure; $\mathbf{\Lambda}$ is an array of control parameters, containing the components of external loading, whereas $\mathbf{r}$ is the residual vector

containing out-of-balance forces, conjugated to **u**. Varying the vector **r** with respect to the components of **u** in the assumption – **Λ**=constant, a tangent stiffness matrix **K** in a structural mechanics application can be written as:

$$\mathbf{K} = \frac{\partial \mathbf{r}}{\partial \mathbf{u}}. \tag{3}$$

An alternative version of equation (2) is the force-balance form:

$$\mathbf{p(u)} = \mathbf{f(u,\Lambda)}. \tag{4}$$

The **p** vector contains components of internal forces, resulting from deformation of the structure; however **f** are the control-dependent external forces, composing the set introduced respectively during the next stages of the analysis, which may also be dependent on the current geometry of the structure.

The philosophy of the nonlinear analysis in FEM is based on the gradual application of control parameters, completed in further stages. It corresponds to the stage for every reliable state of the structure, in which a static balance is specific for a corresponding solution of equation (2). Control parameters connected to external force components are generally expressed as functions of reliable quantity **λ**, called the stage control parameter. The result of the nonlinear analysis, composes a set of solutions, corresponding to each value of the **λ** parameter. They create the equilibrium path of the system. The unambiguous graphical interpretation of the equilibrium path is possible for at most two degrees of freedom. However with the knowledge of external loading, the value of stage control parameters and related geometric structural configurations, it is possible to obtain an approximated dependence between selected values describing deformation of the structure versus external loading. For the numerical models considered, equilibrium paths were determined in the method: torsional moment versus total torsional angle.

Algorithms of nonlinear analysis are mainly based on iterative and incremental – iterative procedures. The stiffness matrix **K** is treated in every equation stage, as a constant and it is increased as far as the **λ** stage control parameter is increaded. The Newton-Raphson algorithm constitutes the basic iterative method. Its' drawback is that it cannot obtain the solution convergence. This method is bound up with the appearance of the limit of bifurcation points on the equilibrium path. In such situations, the arc length method is applied, which makes it possible to determine the balance of the system [4], [5], [6], [14], [15].

Nonlinear, numerical analyses of this problem were done, applying the MSC MARC 2005 programme. This programme allows the user to intervene in the iteration parameter selection.

The same numerical model, which was applied in the linear analysis, was utilized without stiffening stringers as a structure. Two diversified numerical models were analyzed, with the structure stiffened by the stringers of "omega" in the cross section of each. The first has a surface – stringer rivet joint, simulated by beam elements. Contact was also reflected between the surfaces of stringers and the surface itself. A simplification was applied in the second model, relying on the continuous connection of stringers with surface.

After several numerical tests, the boundary conditions of all models were changed, due to their excessive stiffness. The establishment of the back edges of the shells, as shown in Fig. 2 was replaced by ribs with additional supports.

The effects, illustrating the character of deformation in numerical calculations and effective stress distribution on external structural surfaces, are shown by Figs. 14–19.

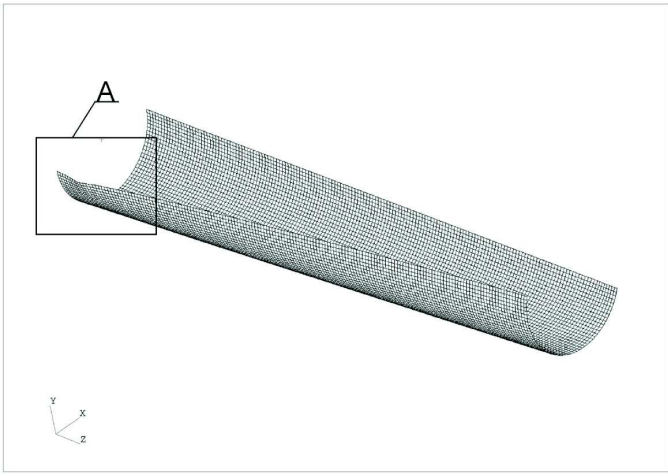

Fig. 14. Post buckling deformation. Structure without stringers

The results of the calculations presented in Figs. 14 and 15, prove the existence of local plastic deformation areas in the vicinity of the boundary fixing of the structure. These effects show satisfactory compatibility with the experiment (compare Fig. 12), both in the location and the character of the plastic deformation range.

Figures 16 and 17 show the numerical results for the model, where the connection was reflected by inner rivets. The result obtained, describing the state of local plastic deformation in a post-buckling state, differs qualitatively from the effect noted in the experiment. Several attempts were made (not presented here) to identify reasons for this divergence. It is possible, on this basis, to make an attempt to explain this phenomena.

Looking at Fig. 17, we can notice that the elements of the surface and stringer in the zone between rivets, were subjected to transverse dislocations,

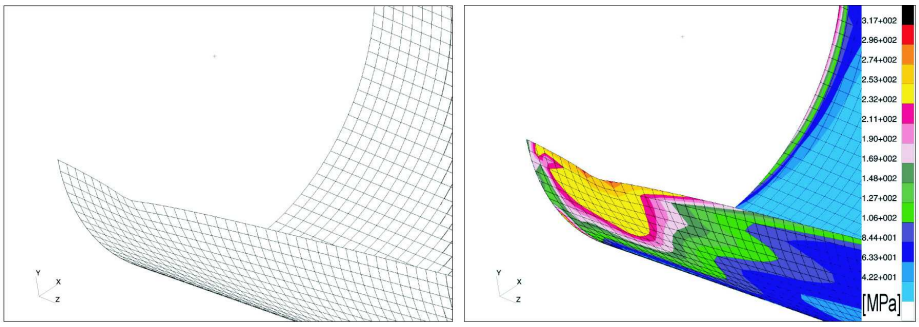

a) b)

Fig. 15. Form of post buckling deformation; a) area of A detail in actual scale; b) effective stress distribution on external surface according to von Mises' criterion

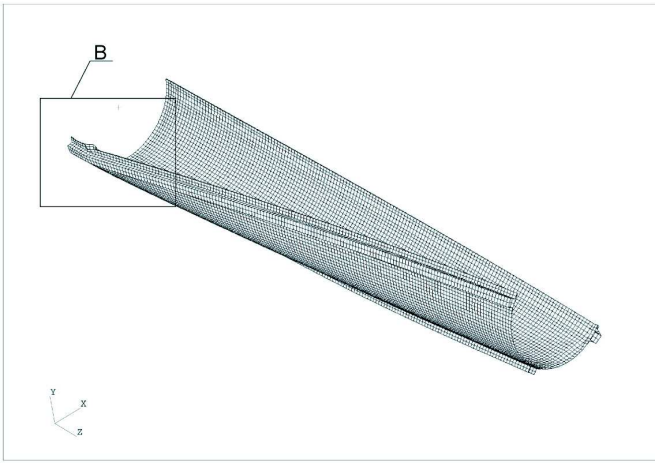

Fig. 16. Version 1-riveted joint of the surface with the stringer. Local post-buckling deformation

moving in opposite directions, while the direction of dislocations were the same. This divergence could be the result of a loss of stability bifurcation. A reasonable suggestion arises from the fact that in both elements the bifurcation had a stable-symmetrical character. In the actual structure, geometric imperfections could determine the identical direction of the dislocation of both surfaces already initiated during the riveting process.

The second model was of considerable interest. The results of numerical calculations correspond exactly to the results of the experiment (Figs. 18, 19). Applied simplifications adjust conditions of the iteration parameters selection in the actual structure transformation. They rely on the continuous connection between stringers and surfaces, which eliminates the possibility of local stress concentration in the proximity of the rivets. Taking into consideration the

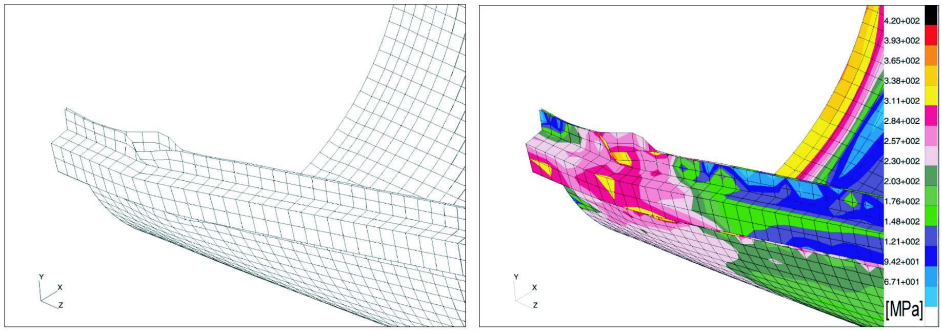

a) b)

Fig. 17. Form of post-buckling deformation; a) area of C detail in actual scale; b) effective stress distribution on external surface according to von Mises' criterion

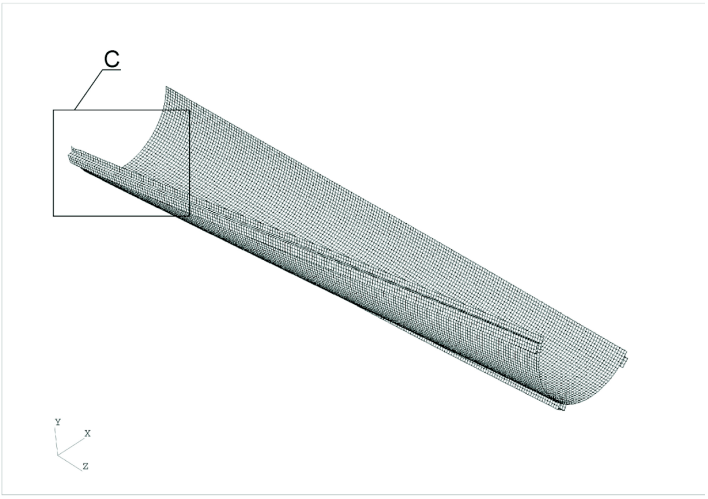

Fig. 18. Version 2 – continuous connection of surface and stringers. Local post-buckling deformation

character of advanced plastic deformation as noted, and the responding stress distribution, it is possible to regard the results obtained as satisfactory.

In Fig. 20, the relationship between the torsion moment and the torsion angle is shown as obtained both in the experiment and in the calculation.

It is necessary to emphasize that the results of the numerical calculations present approximate relations between the loading and the accepted parameter, determining structure deformation. In fact, the obtained characteristics express the relationship between the torsion angle of the structure and the product: $\mathbf{M_{max}} \cdot \mathbf{p_t}$, where $\mathbf{p_t}$ denotes a pseudo-time coefficient, as the step of load advantage application, in the particular, step of counts, whereas $\mathbf{M_{max}}$ is the maximum value of the structure loading. In the case considered, it is

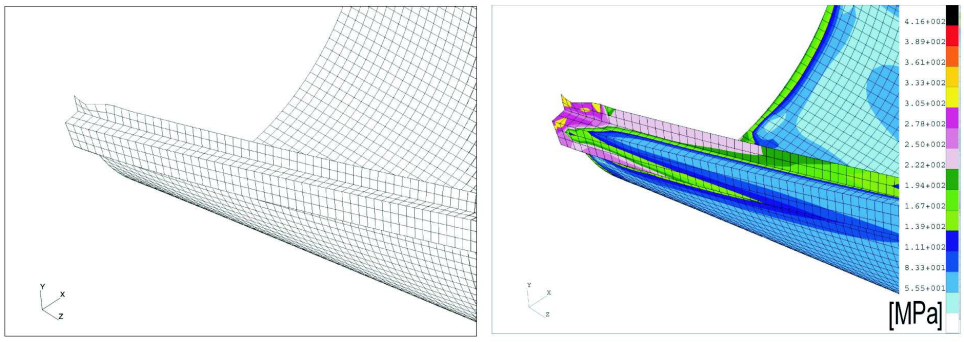

a) b)

Fig. 19. Form of post-buckling deformation; a) area of B detail in actual scale; b) effective stress distribution on the external surface according to von Mises' criterion

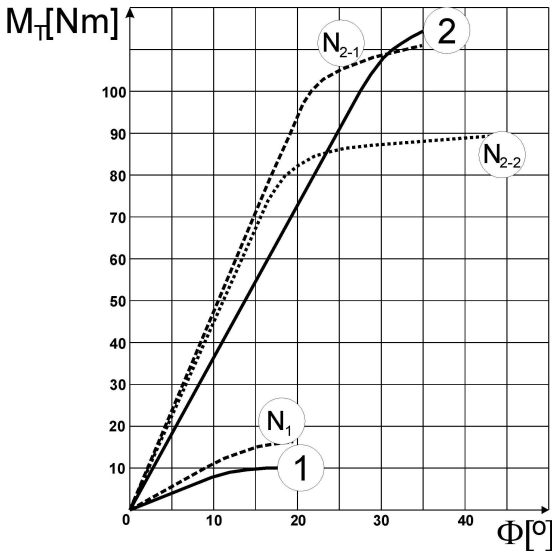

Fig. 20. Relationship between the torsion moment versus the torsion angle.
1 – Structure without stringers – experimental result
2 – Structure reinforced by closed section stiffeners – experimental result
N_1 – Structure without stringers – numerical result
N_{2-1} – Version with continuous connection of surface and stringers – numerical results
N_{2-2} – Version with riveted joint of the surface with the stringers – numerical results

a maximum value of the torsional moment. The relationship is dependent on the accepted method of the solution, the parameters of the iteration, and the shape of the equilibrium path, between the products mentioned above and the actual loading of the numerical model. It should be noted, that the loading of the numerical model is the maximum accepted value of the torsional moment for $\mathbf{p_t = 1}$.

6. Concluding remarks

On the basis of the numerical and experimental results, several statements could be formulated, essential for engineering practice.

- The results obtained numerically show higher critical load values in all considered cases. It is possible that this can be explained by a rather imprecise rigidity, reflecting the actual design in the numerical model, as whole. It is related to the plate boundary conditions, in particular. Additionally, the structure stiffness execution process should be considered.
- Establishing the back edge of the shell by limiting its degrees of freedom causes excessive stiffness in the numerical model of the structure. It is necessary to apply boundary conditions reproducing actual mount flexibility.
- Linearised pre-buckling analysis gives reliable results if the first element of decreasing stability in a complex structure is characterized by little stress redistribution (a stringer, for example).
- The obtained divergence between the nonlinear numerical analysis and the results of the experiments suggests that appropriate imperfections of structure geometry in the numerical model, should be taken into consideration. The effect would be the ability to propose reliable inferences, if not requirements, in relation to the technological process, particularly for neuralgic zones, determining the load capacity of the structure.
- The presented study denotes experimental revision, information about structure behaviour under loading, and a verification function for the numerical FEM model, in particular, where the solution of the problem requires nonlinear formulation.

Manuscript received by Editorial Board, December 19, 2006;
final version, June 04, 2007.

REFERENCES

[1] Arbocz J.: Shell stability analysis: theory and practice. Collapse, the buckling of structures in theory and practice. In: Thompson J. M., Hunt G. W. (editors), Cambridge University Press, 1983.
[2] Bathe K. J.: Finite Element Procedures. Prentice Hall, Upper Saddle River, New Jersey, 1996.
[3] ABACUS Analysis User's Manual, version 6.3.
[4] Crisfield M. A.: A faster modified Newton-Raphson iteration. Comp Meth Appl Mech Engrg 20, 267÷278 (1979).
[5] Crisfield M. A.: Incremental/iterative solution procedure for nonlinear structural analysis in numerical method for nonlinear problems. Vol. 1, (eds. C. Taylor, E. Hinton and D. R. J. Owen), Pineridge Press, Sweansea, 1980.
[6] Crisfield M. A.: An arc-length method including line Searches and accelerations. Int J Num Meth Engrg 19, 1269÷1289 (1983).

[7] Dube G. P., Dumir P. C.: Tapered thin open section beams on elastic foundation – I. Buckling analysis. Comp Struct 61, 845÷857 (1995).
[8] Felippa C. A.: Nonlinear finite element methods. Department of Aerospace Engineering Sciences University of Colorado, Boulder, Colorado 2004.
[9] Kollar L. P.: Flexural – Torsional buckling of open section composite columns with shear deformation. Int J Solids Struct 38, 7525÷7541 (2001).
[10] Królak M., Młotkowski A.: Experimental analysis of post – buckling and collapse behaviour of thin – walled box-section beam. Thin Wall Struct 26, 287÷314 (1996).
[11] Mohri F., Azrar L., Potier-Ferry M.: Flexural – torsional post – buckling analysis of thin – walled elements with open sections. Thin Wall Struct 39, 907÷938 (2001).
[12] Mohri, F., Azrar L., Potier-Ferry M.: Lateral post buckling analysis of thin-walled open section beams. Thin Wall Struct 40, 1013÷1036 (2002).
[13] MSC MARC FE user's manual 2005.
[14] Riks E.: An incremental approach to the solution of Snapping and buckling problems. Int J Solids Struct 15, 329÷351 (1979).
[15] Riks E.: Some computational aspects of the stability analysis of nonlinear structures. Comp Meth Appl Mech Engrg 47, 219÷260 (1984).
[16] Zienkiewicz O. C., Taylor R. L.: Finite element method for solid and structural mechanics. Elsevier Butterworth-Heinemann, 2005.

Analiza wyboczenia oraz stanów deformacji zakrytycznych powłok walcowych, o przekrojach otwartych, poddanych skręcaniu nieswobodnemu

S t r e s z c z e n i e

W pracy zaprezentowano wyniki eksperymentalno-numerycznych analiz deformacji walcowych, otwartych powłok, poddawanych skręcaniu nieswobodnemu, w zakresie obciążeń krytycznych i zakrytycznych. Rozważano dwa warianty struktury. Pierwszy z nich stanowiła powłoka pozbawiona wzmocnień, drugi – powłoka wzmocniona podłużnicami. Analiza numeryczna, w ujęciu metody elementów skończonych, obejmowała pięć ustrojów każdego rodzaju, o różnych długościach. Stosowano zlinearyzowaną analizę wyboczeniową oraz przyrostowo-korekcyjną analizę nieliniową. Obliczenia numeryczne pozwoliły określić rozkłady wytężenia w newralgicznych strefach ustrojów. Ich wyniki porównywane były z rezultatami eksperymentu. Dążono do uzyskania zgodności postaci i wielkości deformacji. Praca zakończona jest szeregiem wniosków i zaleceń konstrukcyjnych.